J. of Supercritical Fluids 49 (2009) 71–78

Contents lists available at ScienceDirect

The Journal of Supercritical Fluids

journal homepage: www.elsevier.com/locate/supflu

Normal-phase dynamic imaging of supercritical-water salt precipitation using neutron radiography

Andrew A. Peterson[a,b], Peter Vontobel[c], Frédéric Vogel[b,*,1], Jefferson W. Tester[a]

[a] Department of Chemical Engineering, Massachusetts Institute of Technology, Cambridge, MA, USA
[b] Laboratory for Energy and Materials Cycles, Paul Scherrer Institut, Switzerland
[c] Spallation Neutron Source Division, Paul Scherrer Institut, Switzerland

ARTICLE INFO

Article history:
Received 12 August 2008
Received in revised form
29 September 2008
Accepted 16 November 2008

Keywords:
Supercritical water
Salt
Neutron radiography
Precipitation
Sodium sulfate
Potassium phosphate
Biomass gasification

ABSTRACT

Although neutron radiography has been effectively used to dynamically image the separation of salts from supercritical water, earlier approaches have relied on an artificial model system that was limited to boron-containing salts in heavy water, D_2O. In this work we demonstrate that similar information may be obtained with the contrasts reversed: boron-free salt buildup can be seen in supercritical H_2O. This new technique enables *in situ* imaging as illustrated by results obtained for systems of interest for biomass gasification, where solid plugging and flow pattern changes were clearly imaged within the vessel. As compared to the D_2O method, the H_2O method does not explicitly distinguish between regions of low water density and buildup of salt; however, the H_2O method can provide information on fluid density changes that the D_2O method does not. This method was applied to determine the behavior of Na_2SO_4 in ^1H_2O, which led to plugging and erratic behavior, and to K_3PO_4 in ^1H_2O, which led to smooth operation. Plugging behavior of Na_2SO_4 was drastically reduced by the addition of K_3PO_4 to the feed, which suggests the formation of a liquid brine.

1. Introduction

Supercritical water provides a medium for high-efficiency reforming of waste biomass streams into useful fuels and chemicals [1]. A catalytic supercritical-water gasification process has been developed at the Paul Scherrer Institut that has demonstrated 99% gasification of 30 wt% wood slurries and representative model solutions to CH_4, H_2 and CO_2[2,3]. However, catalyst stability is an issue and can often be traced to the presence of inorganic species [4]. Further, ionic species frequently precipitate as solids, which, depending on the ions present and the operating conditions, can lead to vessel plugging [5].

Separation technologies for supercritical-water systems exist that take advantage of the drop in the dielectric constant of water as it is heated to near-critical and supercritical conditions [6,7]; one of the more common approaches is to precipitate ions in a reverse-flow vessel. These vessels can be difficult to operate, and validation of computational fluid dynamics models [8–10] has not been possible without flow field measurements and experimental characterization of precipitation behavior inside of these vessels.

In earlier work [11], we showed that neutron radiography could be used to dynamically image the build-up of salts *in situ* in a supercritical-water salt separator. However, our approach was limited to using heavy water (D_2O) as the mobile phase and mixtures with a boron-containing salt as the precipitating phase. This was done for achieving high-contrast: D_2O is relatively transparent to thermal neutrons, as opposed to H_2O which strongly attenuates neutrons by scattering (Or, simply, H_2O is nearly opaque in neutron radiographs and D_2O is nearly transparent). Boron strongly attenuates neutrons, causing boron-containing salts to appear dark on a nearly transparent background in these images, which highlights areas with salt accumulation. We will refer to this approach as "reverse-phase" (RP) imaging. Table 1 lists neutron attenuation coefficients for H_2O, D_2O, and some boron-containing and boron-free salts for neutrons at 1.54 Å.

While the reverse-phase approach allowed us to clearly observe behavior which was not previously accessible, it was limited to artificial systems such as $D_2O/Na_2B_4O_7$. In this paper, we show that the contrasts can be reversed, thus allowing *any* salt to be observed precipitating and accumulating from supercritical ^1H_2O, in what we will refer to as "normal-phase" (NP) imaging. This concept is illustrated in Fig. 1. While the NP technique does not allow us to see smaller precipitation events that were visible with the RP approach, it does identify the events and regimes in which plugging and flow changes in the vessel occur. Further, as we will show, water density changes are apparent with the NP approach, allow-

* Corresponding author at: Laboratory for Energy and Materials Cycles, Paul Scherrer Institut, CH-5232 Villigen PSI.
E-mail addresses: aap@mit.edu (A.A. Peterson), frederic.vogel@psi.ch (F. Vogel).
[1] Tel.: +41 56 310 2135.

0896-8446/$ – see front matter © 2008 Elsevier B.V. All rights reserved.
doi:10.1016/j.supflu.2008.11.019

Table 1
Neutron attenuation coefficients at 1.54 Å. Data from Sears [19].

Material	Attenuation coefficient (cm^{-1})
Water:	
H_2O	5.39 [a]
D_2O	0.124 [a]
Salts:	
Na_2SO_4	0.029 [b]
K_3PO_4	0.031 [b]
$Na_2B_4O_7$	13.66 [b]
Materials of construction:	
Zircaloy-2	0.009 [c]
Aluminum	0.012 [d]

[a] At 1.00 g/cm³.
[b] At 1.73 g/cm³.
[c] At 6.56 g/cm³.
[d] At 2.70 g/cm³.

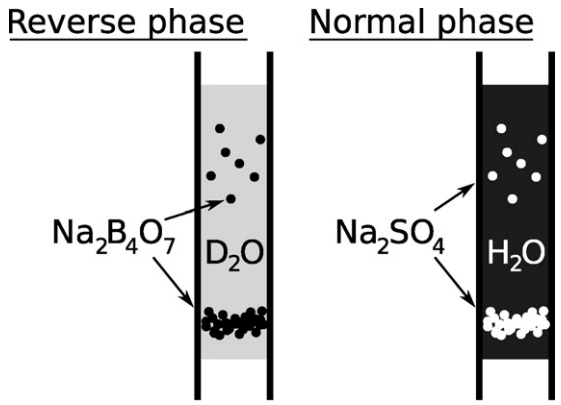

Fig. 1. Illustration of the phase reversal employed in this experiment. The left-hand figure shows the approach taken previously [11]: borax, which appeared opaque, was used as a tracer in supercritical D_2O, which appeared transparent, giving high contrast and allowing us to see small precipitations of salts as well as plugging. In the current work, illustrated on the right, boron-free salts such as Na_2SO_4 appear transparent while supercritical H_2O appears opaque.

Table 2
Comparison of reverse-phase and normal-phase methods employed.

	Reverse-phase (RP)	Normal-phase (NP)
Liquid phase	D_2O	^1H_2O
Salt	Boron-doped, such as Na_2SO_4 with $Na_2B_4O_7$	Without boron, such as K_3PO_4 or Na_2SO_4
Neutron energy (most probable)	~ 25 meV	~ 25 meV
Observable phenomena	Small and large salt precipitation	Large salt precipitation, fluid density changes

ing flow pattern changes to be visible that would not be seen with the RP technique. Table 2 summarizes the differences in the two methods.

2. Materials and methods

The apparatus was identical to what we reported earlier [11]; the main difference was that ^1H_2O (not D_2O) was used as the mobile phase and K_3PO_4 and Na_2SO_4 were used as the precipitating phases (without $Na_2B_4O_7$).

2.1. Imaging with neutron radiography

Neutron radiographs were acquired at the thermal neutron radiography facility NEUTRA (http://neutra.web.psi.ch/) of the Paul Scherrer Institut, Villigen, Switzerland, which is described in more detail by Lehmann et al. [12] but summarized here. The

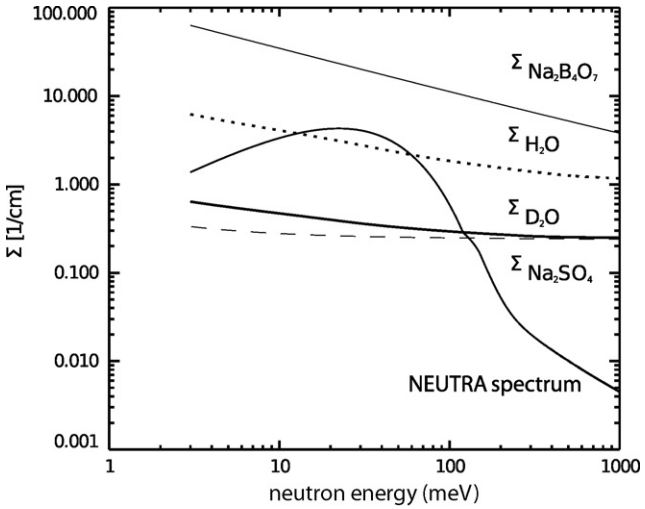

Fig. 2. The energy spectrum at NEUTRA. Superimposed are the linear attenuation coefficients of light and heavy water at 30 MPa and 300 °C. Values for salts given for comparison at room temperature and nominal solid density. The effective spectrum averaged Σ values for an 8-mm thick water layer are about 0.38 cm^{-1} for heavy water and 2.76 cm^{-1} for light water. Note that $\Sigma_i = \sigma_i \rho_i N_A / M_i$.

energy spectrum of the neutrons at NEUTRA is a polychromatic, Maxwellian energy spectrum with most probable energy at about 25 meV as shown in Fig. 2. The neutron flux at the sample position was 3.9×10^6 neutrons $cm^{-2}\,s^{-1}$. The collimation ratio [13] L/D describing beam divergence was 550, inducing a geometrical unsharpness of about 120 μm. Radiographs were recorded with a Peltier-cooled (−45 °C) slow-scan CCD camera featuring a 1024 × 1024 pixel chip (camera type DV 434, Andor Technology, www.andor-tech.com). Neutron flux was converted into light with a Li-6 doped ZnS screen with thickness 250 μm. The field of view captured by a 50 mm Pentax F 1.2 normal lens was 90 mm × 90 mm, representing a nominal pixel size of 88 μm × 88 μm at full resolution and 176 μm × 176 μm after binning 2 × 2 pixels. The effective spatial resolution [14], however, was limited by the scintillator thickness to about 400 μm/pixel. The exposure time was 15 s per picture providing a dynamic range of about 25,000 gray levels. This exposure time allowed for the visualization of salt accumulation, which generally occurred over the timespan of a few minutes.

2.1.1. Image analysis

Each 15-s neutron radiography exposure produced a 512 × 512-element matrix of intensity data proportional to neutron transmission at each point on the grid. These values were converted to relative transmission by dividing each element in the matrix by the "flatfield" transmission, or transmission when no sample was present in the field of neutrons. This conversion provided values described by the Beer–Lambert exponential attenuation law,

$$\frac{I(\vec{r})}{I_0(\vec{r})} = \exp\left\{ - \sum_{i=1}^{\#\,\text{materials}} \frac{\rho_i}{M_i} N_A \sigma_i \Delta x_i(\vec{r}) \right\}$$

where $I(\vec{r})$ is the intensity of neutrons passing through the sample at point $\vec{r}$, $I_0(\vec{r})$ is the neutron intensity entering the sample at point $\vec{r}$, ρ_i, M_i, and σ_i are the density, molecular weight, and neutron attenuation coefficient of material i, $\Delta x_i(\vec{r})$ is the thickness of material i at position $\vec{r}$, and N_A is Avogadro's number. In this way, materials with different attenuation coefficients (σ_i) can be distinguished by the intensity of neutrons passing through a sample. In particular, lightly attenuating materials such as Na_2SO_4 were distinguishable from strongly attenuating materials such as H_2O. H_2O attenuates neutrons by scattering. Scattered neutrons can reach the detec-